Interface equations for capillary rise in random environment

T. Laurila, C. Tong,* S. Majaniemi,† and T. Ala-Nissila‡
Laboratory of Physics, P.O. Box 1100, Helsinki University of Technology, FIN-02015 HUT, Finland
(Received 20 January 2006; published 13 October 2006)

We consider the influence of quenched noise upon interface dynamics in two-dimensional (2D) and 3D capillary rise with rough walls by using a phase-field approach, where the local conservation of mass in the bulk is explicitly included. In the 2D case, the disorder is assumed to be in the effective mobility coefficient, while in the 3D case we explicitly consider the influence of locally fluctuating geometry along a solid wall using a generalized curvilinear coordinate transformation. To obtain the equations of motion for meniscus and contact lines, we develop a systematic projection formalism that allows inclusion of disorder. Using this formalism, we derive linearized equations of motion for the meniscus and contact line variables, which become local in the Fourier space representation. These dispersion relations contain effective noise that is linearly proportional to the velocity. The deterministic parts of our dispersion relations agree with results obtained from other similar studies in the proper limits. However, the forms of the noise terms derived here are quantitatively different from the other studies.

DOI: 10.1103/PhysRevE.74.041601 PACS number(s): 68.08.−p, 46.65.+g, 68.35.Ct, 05.40.−a

I. INTRODUCTION

The dynamics and roughening of moving interfaces in disordered media has been a subject of great interest in nonequilibrium statistical physics since the 1980s. Relevant examples of physically and technologically important processes include thin-film deposition [1], fluid invasion in porous media [2–4], and wetting and propagation of contact lines between phase boundaries [5–7]. The understanding of the underlying physics involved in interface roughening is crucial to the control and optimization of these processes. Significant progress in the theoretical study of interface dynamics has been made and a number of theories have been developed [8], which in some selected cases agree well with the experimental findings [9]. Most of the theoretical understanding in this field is based on modeling interface roughening with a local stochastic equation of motion for the single-valued height variable of the interface. However, there are several cases of interest in which such an approach cannot be justified, e.g., due to conservation laws in the bulk. This is especially true for processes such as fluid invasion in porous media, which is often experimentally studied by Hele-Shaw cells [10–12], or imbibition of paper [13–15]. It has been shown that in such cases, spatially local theories cannot provide a complete description of the underlying dynamics. For describing the diffusive invasion dynamics in such systems, a phase-field model explicitly including the local liquid bulk mass conservation law has been developed and applied to the dynamics of one-dimensional (1D) imbibition fronts in paper [16]. This was achieved by a generalized Cahn-Hilliard equation with suitable boundary conditions, which couple the system to the reservoir. Numerical results for roughening from the model are in good agreement with relevant experiments [17].

One of the great advantages of the phase-field approach is that it is possible to analytically derive equations of motion for the phase boundaries in the so-called sharp interface limit [18]. Most recently, we have developed a systematic formalism to derive such equations for the 2D meniscus and 1D contact line dynamics of fluids in capillary rise [19]. The equations are derived from the 3D bulk phase-field formulation, using a variational approach as applied to relevant Rayleigh dissipation and free-energy functionals. Through successive projections, equations of motion for the 2D meniscus and 1D contact line can be derived. The leading terms of such equations (for small-amplitude, long-wavelength fluctuations) can be shown to agree with results obtained from the sharp interface equations in the appropriate limits [20].

In addition to the need for nonlocal models to account for mass conservation, in Hele-Shaw and imbibition problems the inherent quenched disorder should be properly taken care of. Unlike thermal disorder, which is relatively easy to handle, quenched disorder depends on the height of the 1D interface $h(x,t)$ as $\eta(x,h(x,t))$. This makes its influence on interface roughening highly nontrivial, often leading to anomalous scaling [21,22]. Currently, for such cases good agreement between theory, simulations, and experiments has not been achieved. Even on the experimental side, some results, such as the quantitative values of the scaling exponents, are not consistent and difficult to interpret. Very recently, Soriano *et al.* [10] conducted an experimental study of forced fluid invasion in a specially designed Hele-Shaw cell. The quenched disorder pattern in the Hele-Shaw cell is realized by creating a large number of copper islands that randomly occupy the sites of a square grid on a fiberglass substrate fixed on the bottom Hele-Shaw cell. Three different disorder patterns were used. Two of them are obtained by random selection of the sites of a square lattice. The third kind of disorder is formed by parallel tracks, continuous in the interface growth direction and randomly distributed

*Present address: Department of Materials Science and Engineering, McMaster University, Hamilton, Ontario, Canada.
†Present address: Department of Physics, McGill University, 3600 University Street, Montréal, QC, Canada H3A 2T8.
‡Also at Department of Physics, Brown University, Providence RI 02912-8143.

along the lateral direction. It was found that for forced flow, the temporal growth exponent $\beta \approx 0.5$, which is nearly independent of experimental parameters and disorder patterns. However, the spatial roughness exponent χ was found to be sensitive to experimental parameters and disorder patterns. Anomalous scaling with $\chi \approx 1.0$ and a local roughness exponent $\chi_{\mathrm{local}} \approx 0.5$ were found in the disorder pattern with parallel tracks along the growth direction. It was also demonstrated that such anomalous scaling is a consequence of different local velocities on the tracks and the coupling in the motion between neighboring tracks.

On the theoretical side, for nonlocal Hele-Shaw and paper imbibition problems there are two different approaches within the phase-field models to include additive quenched disorder. Dubé *et al.* [16,17] put the quenched disorder inside the chemical potential, the gradient of which is the driving force for interface motion. On the other hand, Hernández-Machado *et al.* [23] accounted for the effect of fluctuation of Hele-Shaw gap thickness as a mobility with quenched disorder in the phase-field model, while keeping the chemical potential free of noise. These two approaches lead to quantitatively different roughening properties. This issue has been considered in terms of a general porous structure by Dubé *et al.* [24]. In terms of a fluctuating gap in a Hele-Shaw cell, these disorder types were considered by Pauné and Casademunt [11] with a model that took different effective noise contributions into account. They discovered that a length scale determines the crossover between capillary noise, which is like that of Dubé *et al.* [16], and permeability noise, which is like that of Hernández-Machado *et al.* [23]. According to these results, fluctuating gap experiments such as [10] fall under the domain in which capillary noise dominates.

When considering the problem of capillary rise in a typical Hele-Shaw cell setup between two rough walls more microscopically, the location of the surface of such corrugated walls in the Cartesian coordinate system is a spatially fluctuating quantity, which indicates the presence of quenched disorder. An experimental realization is given in [12]. To treat this problem faithfully, in solving the phase-field equation such a fluctuating wall surface should be treated as a physical boundary without phenomenologically adding quenched noise to the equation of motion, as done previously. Consequently, it is evident that a rigorous analytic treatment of such a problem is overwhelmingly difficult. However, in this paper we demonstrate that with proper mathematical formulation of the problem, it is possible—albeit with some approximations—to analytically derive equations of motion for the meniscus and contact line dynamics. Most importantly, these equations incorporate the wall disorder in a natural way. To achieve this, we utilize an explicit curvilinear coordinate transformation of the phase-field equation in order to apply projection methods to unravel the relevant physics in the limit of small disorder. To some extent, this kind of curvilinear coordinate transformation is similar to the boundary-fitted coordinate system frequently used in computational fluid dynamics (CFD) [25].

The outline of this paper is as follows. In Sec. II, we will consider the phenomenological 2D phase-field model of capillary rise with quenched disorder in the mobility, similar to that in Refs. [23,26]. We will adapt the systematic projection method of Kawasaki and Ohta [27] to obtain a linearized interface equation (LIE) that describes small fluctuations of an interface, whose deterministic part reduces to the previous result [23,26] in a special limit. To treat the problem rigorously, in Sec. III we will consider the full 3D phase field model with corrugated walls as the source of quenched disorder. The transformation to curvilinear coordinates, as discussed above, is introduced to obtain linearized, effective bulk disorder from the original curvilinear boundary condition. Following this, we develop and apply a general projection scheme [19] to obtain the effective equations of motion for small fluctuations of the 2D meniscus, and ultimately for the 1D contact line between the meniscus and the wall. Again, the deterministic parts of these equations reduce to previously known limits in special cases. However, we demonstrate that the forms of the quenched noise terms derived here are different from the previous works.

II. 2D PHASE-FIELD MODEL WITH STOCHASTIC MOBILITY

A 2D phase-field model explicitly including the local conservation of bulk mass was introduced to study capillary rise by Dubé *et al.* [16]. The bulk disorder in their model was included in the effective chemical potential. Recently a similar model, where the disorder was considered through a stochastic mobility coefficient, was studied by Hernández-Machado *et al.* [23,26]. In particular, they assumed a one-sided mobility coefficient, which vanishes on one side of the interface. From this model, they derived an equation of motion for small interface fluctuations. In this section, we will use the systematic projection method introduced by Kawasaki and Ohta [27] to derive the corresponding linearized interface equation (LIE) describing small fluctuations in a sharp interface in a similar model. In our model, we assume the mobility to be independent of the phase, as in the previous works [16], but spatially stochastic, as in [23,26]. This corresponds to considering the invading fluid and the porous medium, but not the receding fluid. This picture is valid when the receding fluid has low density and viscosity. In practice, this would mean a gas, such as air, being displaced by a liquid, such as water or oil. The model allows a systematic projection of the effective noise term at the interface.

The phase-field model describes capillary rise at a coarse-grained level with a phase field $\phi(\mathbf{x},\mathbf{t})$ that obtains the value $\phi=-1$ in the phase of the displaced fluid, and $\phi=+1$ in the phase of the displacing fluid. The phase field thus describes the effective component densities, and thus must be locally conserved. An energy cost for an interface is included to obtain the free energy in dimensionless units as

$$\mathcal{F}[\phi(\mathbf{x},t)] = \frac{1}{2}[\nabla\phi(\mathbf{x},\mathbf{t})]^2 + V(\phi(\mathbf{x},\mathbf{t})), \tag{1}$$

where V has two minima at $\phi=+1$ and -1. The details of V are not relevant in the sharp interface limit, except to define the surface tension, so we can choose the standard Ginzburg-Landau form $V(\phi)=-\phi^2/2+\phi^4/4-\alpha\phi$, where one of the phases can be set metastable by nonzero coefficient α. The

equation of motion for the conserved phase field is given by the continuity equation $\partial_t\phi=-\nabla\cdot\mathbf{j}$ and Fick's law $\mathbf{j}=-\tilde{M}\nabla\mu$, where $\mu=\delta\mathcal{F}/\delta\phi$, and $\tilde{M}=M[1+\xi(x)]$ is the mobility that we choose to be a position-dependent stochastic variable here. The resulting equation of motion for the phase field is then given by

$$\partial_t\phi(x,t)=\nabla\cdot\tilde{M}(x)\nabla\mu[\phi]$$
$$=M\nabla\cdot[1+\xi(x)]\nabla[V'(\phi)-\nabla^2\phi], \qquad (2)$$

where the variable ξ is now the dimensionless, quenched noise. The sharp interface limit of this model without the noise is well known, and discussed, e.g., in Ref. [18]. The geometry of the problem is that of a half-plane, where a reservoir of the displacing fluid is located at the x axis. The boundary condition of the chemical potential at the half-plane boundary can be connected to the physical effect that is driving the capillary rise. In this paper, we will consider spontaneous imbibition, where the rise is driven by a chemical potential difference in the medium, which favors the displacing fluid [16]. This means that the two minima of V are at different heights. In our notation, the chemical potential difference is 2α, and we consider a chemically homogeneous medium, where α=const. Spontaneous imbibition corresponds to a Dirichlet boundary condition (μ=const=0) at the reservoir [16]. Forced flow, where flow is caused by an imposed mass flux into the system from the reservoir, can be modeled with the Neumann boundary condition ($\nabla\mu=F\hat{y}$), where F is the flux [17]. An analysis along the lines presented in this paper can also be conducted for the case of forced imbibition. A recent review of phase-field modeling of imbibition is given in Refs. [28,29].

Using the Green's function $G(r;r')$ for the 2D Laplacian, Eq. (2) can be inverted using Gauss's theorem. This leads to the integro-differential form

$$\frac{1}{M}\int_V dr'\sqrt{\det(g')}G\partial_t\phi'$$
$$=(1+\xi)\mu-\int_V dr'\sqrt{\det(g')}G\nabla'\xi'\cdot\nabla'\mu'$$
$$-\int_V dr'\sqrt{\det(g')}G\mu'\nabla'^2\xi'+\Lambda. \qquad (3)$$

Notation here has been shortened by omitting the function arguments, and using unprimed and primed functions for functions of unprimed and primed coordinates, respectively. The Green's functions always take both primed and unprimed coordinates as argument. Also the coordinate invariant form is used, with integration measure given by $\sqrt{\det(g)}$. The boundary term Λ vanishes in the case of spontaneous imbibition, or Dirichlet boundary condition in half-plane geometry.

Using the standard 1D kink solution method for projection to sharp interface [27,30] in normal coordinates gives Eq. (3) as

$$\frac{1}{M}\int du\partial_u\phi_0\int ds'du'\sqrt{\det(g')}G\partial_t\phi'$$
$$=-(1+\xi|_{u=0})\left(\sigma\kappa+\int du\partial_u\phi_0\alpha\right)$$
$$+\int du\partial_u\phi_0\int ds'du'\sqrt{\det(g')}G[\partial_{u'}\xi'\partial_{u'}\mu'$$
$$+(1-2u'\kappa')\partial_{s'}\xi'\partial_{s'}\kappa'\partial_{u'}\phi_0']$$
$$+\int du\partial_u\phi_0\int ds'du'\sqrt{\det(g')}G\nabla'^2\xi'(\kappa'\partial_{u'}\phi_0'+\alpha), \qquad (4)$$

where the normal coordinates (s,u) are distances along and perpendicular to the interface, respectively, κ is the local curvature of the interface, $\sigma=\frac{1}{2}\int du[\partial_u\phi_0(u)]^2$ is the surface tension of the phase-field model, and finally ϕ_0 is the 1D kink solution $\partial_u^2\phi_0(u)=V'(\phi_0)$. In the Ginzburg-Landau form of V, this would be given by $\phi_0(u)=\tanh(u/\sqrt{2})$, with the appropriate choice of dimensionless units. We have assumed a disorder correlation length that is larger than the interface width, which leads to the constant surface tension obtained.

With two further approximations [34], the standard procedure [30] can be followed. Transforming the equation to Cartesian coordinates is made somewhat more tedious by the necessity to transform derivatives with respect to s and u, but standard differential geometry methods can be applied. After the sharp interface limit, i.e., $\phi_0\to-1+2\Theta(u)$, the transformation to Cartesian coordinates, and linearization in small fluctuations of the interface h and the noise ξ, which also eliminates cross terms proportional to $h\xi$, we get the LIE as

$$\frac{1}{M}\int dx'[G(x,H_0;x',H_0)+\partial_y G(x,y;x',H_0)|_{y=H_0}h(x,t)$$
$$+\partial_{y'}G(x,H_0;x',y')|_{y'=H_0}h(x',t)]\partial_t[H_0(t)+h(x',t)]$$
$$=-\sigma\partial_x^2h(x,t)-\alpha+\frac{\partial_tH_0(t)}{M}\Xi(x,H_0(t)), \qquad (5)$$

where the disorder term Ξ is given by

$$\Xi(x,y)=\int dx'\int_0^y dy'\xi(x',y')\partial_{y'}G(x,y;x',y'). \qquad (6)$$

Note that the linearization has been carried out in full here. This means that the disorder term does not include any dependence on the interface fluctuations. This eliminates the nonlinearity of the quenched noise, which is one of its characteristic properties, but we believe it is not crucial in the regime where the linearization is appropriate. In other words, our results show nontrivial features that arise in the effective noise at the interface level with this type of multiplicative bulk disorder, even in the linear regime of weak disorder.

The Green's function for the Dirichlet boundary condition in half-plane geometry is explicitly given by

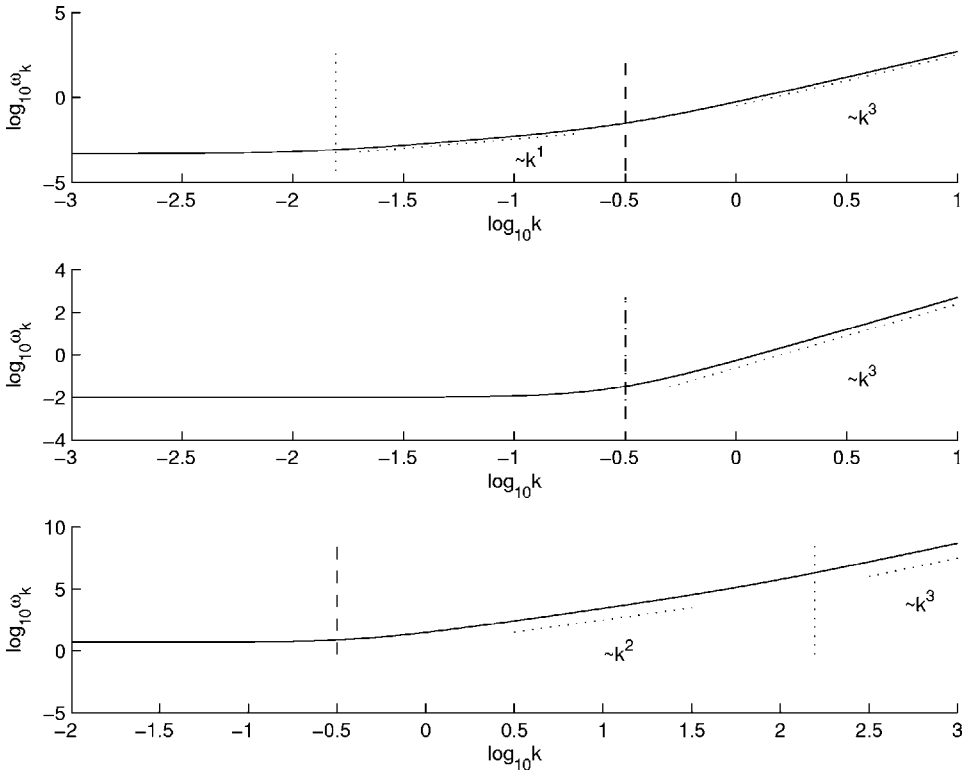

FIG. 1. The dispersion relation in Eqs. (8), (28), and (47) in arbitrary units. The dispersion is determined by the two length scales ξ_x (vertical dashed line) and H_0 (vertical dotted line). The upper figure focuses on the "deep" regime, with $H_0 \gg \xi_x$; in the middle figure these length scales are the same; and the lowest figure focuses on the "shallow" regime, with $\xi_x \gg H_0$.

$$G(x,y;x',y') = \frac{1}{4\pi} \ln \frac{(x-x')^2 + (y-y')^2}{(x-x')^2 + (y+y')^2}. \tag{7}$$

Using this, the Fourier space representation of the interface equation (5) becomes

$$(1 - e^{-2|k|H_0(t)})\partial_t h(k,t) + |k|\partial_t H_0(t)(1 + e^{-2|k|H_0(t)})h(k,t)$$
$$= -\sigma_B |k|^3 h(k,t) + |k|\partial_t H_0(t)\Xi(k,H_0(t)) + |k|M\alpha_k, \tag{8}$$

where $\sigma_B = M\sigma$, α_k is the Fourier transform of the chemical potential difference ($\alpha_k = 0$ if $k \neq 0$, when $\alpha = \text{const}$), and the disorder in Fourier space is given by

$$\Xi(k,y) = -\frac{1}{2}\int_0^y dy' \xi(k,y')(e^{-|k|(y+y')} + e^{-|k|(y-y')}). \tag{9}$$

In the case of columnar disorder, which does not depend on y, the interface equation simplifies to

$$\partial_t h(k,t) = -\frac{|k|\partial_t H_0(t)(1 + e^{-2|k|H_0(t)}) + \sigma_B |k|^3}{1 - e^{-2|k|H_0(t)}} h(k,t)$$
$$+ \partial_t H_0(t)\xi(k) + \frac{|k|M\alpha_k}{1 - e^{-2|k|H_0(t)}}. \tag{10}$$

It is noteworthy that in the limit $k \to 0$, the interface equation is $2H_0(t)\dot{H}_0(t) = M\alpha_0$, readily giving the correct Washburn law [16], if we associate $\lim_{k\to 0} h_k(t) = H_0(t)$ and $\lim_{k\to 0}\alpha_k = \alpha_0$ [35]. Our method of analysis can be applied to the case of forced flow by simply changing the boundary condition of the phase-field model at the reservoir, and applying the corresponding Green's function [17].

The dispersion relation (8) above is the main result in this section. It involves two length scales: a crossover length scale $\xi_x = 2\pi\left(\frac{\sigma}{\dot{H}_0}\right)^{1/2}$ [16] and the distance from the reservoir H_0. The deterministic part of the dispersion relation is plotted in Fig. 1, at the two limits of these length scales: The limit $H_0 \gg \xi_x$ brings out the "deep" limit, $kH_0 \gg 1$, behavior. The limit $\xi_x \gg H_0$ shows the "shallow" limit, $kH_0 \ll 1$, behavior. A plot from the intermediate regime with $H_0 = \xi_x$ is also shown.

The deterministic part of the dispersion relation here is identical to that previously obtained by Dubé *et al.* [16] for the case of disorder in the chemical potential. In the "deep" limit where $\partial_t h = -(\sigma_B |k|^3 + \dot{H}_0 |k|)h$, our result also reproduces that of Hernández-Machado *et al.* [23] for the one-sided mobility case. Using different methods, the same result has also been obtained for the Hele-Shaw setup by Pauné and Casademunt [11] and Ganesan and Brenner [31]. Quadratic nonlinearities in the deterministic part of the dispersion relation have been considered in Refs. [11,31], and these could be added to our calculation. Our focus is on the effective noise terms, however, and for simplicity we have left out all nonlinearities. Note that the LIE is still nonlocal even though it is linearized in fluctuations.

Our noise term in the LIE is similar to those obtained in Refs. [11,23,31] in the sense that in all cases there are effective noise terms, which are linearly proportional to the velocity of the interface propagation. However, the quantitative forms of the noise terms are different when using different methods. How these differences influence the kinetic roughening of interfaces would need to be determined by extensive numerical comparison between the different results, which at this point has not been conducted. As a linear $|k|$ proportionality in the Fourier space representation of the effective noise term is linked to the y derivative of the Green's function of the Laplacian in real-space representation, it appears to us that the linear $|k|$ is present in the appropriate noise terms of

Refs. [31,11], but not in Ref. [23]. The linear $|k|$ dependence is in general characteristic of effective interface noise caused by conserved bulk disorder [16]. However, the $|k|$ dependence $[|k|\partial_t H_0 \Xi(k,H_0(t))]$ dimensionally cancels the integral over the kernel in the effective noise, Eq. (9). This is explicit in the case of columnar disorder in Eq. (10), but is equally valid with the noise in the noncolumnar case. Thus the multiplicative bulk disorder in the mobility leads to a different type of effective noise from that in the chemical potential disorder, which is considered in [16]. Dimensionally this can be seen from the definition of the model, Eq. (2), where the noise term is in front of the gradient of the chemical potential.

The issue of conserved versus nonconserved noise, or equivalently capillary versus permeability noise, was considered in Ref. [11]. In the columnar noise limit, our mobility noise term agrees fully with their permeability noise term. Strictly speaking, this limit is appropriate only when we consider wavelengths much shorter than the disorder correlation length. For large wavelengths comparable to, or larger than, the disorder correlation length, the nontrivial nature of the effective noise in Eq. (9) becomes relevant. Our effective noise term is not easily analyzed, however. In the long-wavelength limit we can consider $\xi(x,y)$ as spatially white noise, i.e., $\langle \xi(\mathbf{r})\xi(\mathbf{r}')\rangle = D\delta(\mathbf{r}-\mathbf{r}')$. We then obtain effective noise that is proportional to $|k|^{1/2}$, which is qualitatively the same as the long-range noise in Ref. [11]. Hence, the 2D mobility noise of Eq. (9) seems to have features of both the permeability and bulk noises of Pauné and Casademunt depending on the length scales. In the case of this 2D phase-field model, the capillary noise term of Pauné and Casademunt does not show up, as expected.

The fact that the columnar disorder leads to effective noise, which is local in Fourier space, is in accordance with the conclusions of experiments of Soriano *et al.* [10], and with the numerical results from the one-sided model [23]. This would indicate that the phase dependence of the mobility is not crucially important when considering the invasion of a viscous fluid into a fluid with negligible viscosity, and when the interface is consequently always stable. When the direction of the invasion is reversed, as studied recently with the one-sided model in [26], the situation is naturally quite different.

III. 3D PHASE-FIELD MODEL WITH FLUCTUATING WALLS

While the stochastic mobility case of the previous section is heuristically appealing, a more faithful treatment of the wall disorder should start from the microscopic roughness of the walls. To this end, in this section we will study a 3D version of the same phase-field model as the 2D model, but where the mobility is constant and the disorder is explicitly included as fluctuations of the wall position. Thus the geometry of the model is that of a Hele-Shaw cell: the 3D volume between two walls that are planar on average, but fluctuate. We will show here that by proper mathematical formulation this model can indeed be analyzed by a generalized projection formalism [19]. The basic idea is to perform a mathematical transformation from the basic Cartesian to a local curvilinear coordinate system as defined by the wall itself. To this end, we consider the one-wall setup as shown in Fig. 2. The one-wall setup neglects the meniscus-mediated interaction between the two contact lines at the two walls. The one-wall approximation also neglects finite gap spacing, i.e., the distance between the two walls in the Hele-Shaw cell, which fluctuates as a result of the wall fluctuations. This induces additional disorder effects when the wall fluctuations are comparable to the gap spacing, but it remains to be studied if the gap effect can be separated from the contact line interaction, which would be represented by two coupled equations of motion for the two contact lines. In the present work, we only consider to the one-wall approximation, or the limit of large gap spacing. Disorder at the wall surface is taken into account by describing local corrugations in the wall position around $y=0$ by a (small) function $y=\delta Y(x,z)$. The explicit coordinate transformation to the local, curvilinear wall coordinate system is defined by

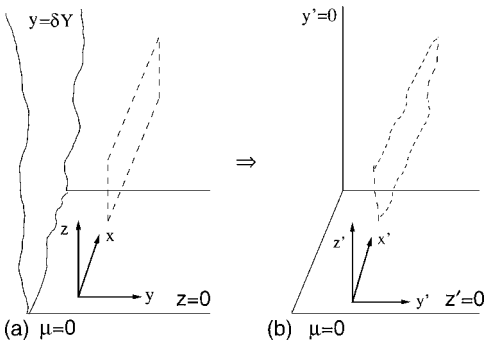

FIG. 2. A schematic presentation of the curvilinear coordinates considered in the Appendix. When presented in terms of curvilinear coordinates, the rough wall by definition looks straight. However, the shift has introduced a coordinate fluctuation in space, where a previously rectangular object looks curved when presented in terms of the new coordinates. This gives rise to a bulk representation of the fluctuating wall, which can be analyzed more easily than the original boundary condition representation.

$$x' = x, \quad y' = y - \delta Y(x,z), \quad z' = z, \tag{11}$$

which corresponds to $y'=0$ when $y=\delta Y(x,z)$. This means that in the new coordinate system the wall is located back at $y'=0$. Given the proper Green's function, $\mathcal{G}$, the phase-field equation can be inverted in any geometry and coordinate system as

$$\frac{\partial \phi}{\partial t} = M\nabla^2\mu \Rightarrow \frac{1}{M}\int dV_1 \mathcal{G}(r,r_1)\frac{\partial \phi(r_1)}{\partial t} = \mu(r) + \Lambda_S, \tag{12}$$

where Λ_S is the corresponding surface term and dV_1 is the volume element for the coordinate system. The Green's-function appropriate for the above-mentioned coordinate system is considered in some detail in the Appendix. Here we compute the correction to the original Cartesian Green's function to linear order in $\delta Y(x,z)$. The final result we obtain, after neglecting some surface contributions that are dis-

cussed in more detail in Appendix , is what one would expect by simply plugging the above definitions into the Cartesian Green's function and linearizing in δY,

$$\tilde{G}_{3D}(\boldsymbol{r}_1;\boldsymbol{r}_2) = G_{3D}(\boldsymbol{r}_1;\boldsymbol{r}_2) - \delta Y(\boldsymbol{r}_1)\partial_{y_1} G_{3D}(\boldsymbol{r}_1;\boldsymbol{r}_2) - \delta Y(\boldsymbol{r}_2)\partial_{y_2} G_{3D}(\boldsymbol{r}_1;\boldsymbol{r}_2). \quad (13)$$

Here G_{3D} is the Green's function for the Laplacian in 3D Cartesian coordinates as given in Eq. (A4). Here again we only consider spontaneous capillary rise, where the boundary conditions for the phase-field model are zero chemical potential at the reservoir and zero flux at the walls. Thus the surface integral term in Eq. (12) is identically zero.

A. Meniscus dynamics

The projection and linearization of the integral equation follows the standard projection operation theory [27,30,32], which we already used in the previous section for the 2D model. The generalization for the present case is straightforward. After projection, the integral equation is expressed in terms of the 2D meniscus variable $H(x,y)$ and has the following form:

$$\int dx'dy' \tilde{G}_{3D}(x,y,H(x,y;t);x',y',H(x',y';t)) \frac{\partial H(x',y')}{\partial t} = \sigma_B \kappa. \quad (14)$$

When linearizing the above equation, it must be done simultaneously in the meniscus fluctuations, i.e., $H(x,y;t) \simeq H_0(t) + h(x,y;t)$, and in the wall fluctuations using the linearized Green's function of Eq. (13). This results in the linearized Green's function evaluated at the meniscus,

$$\begin{aligned}\tilde{G}_{3D}(x,y,H(x,y);x',y',H(x',y')) &\simeq G_{3D}(x,y,H_0;x',y',H_0) \\ &+ \delta Y(x,H_0)\partial_y G_{3D}(x,y,H_0;x',y',H_0) \\ &+ \delta Y(x',H_0)\partial_{y'} G_{3D}(x,y,H_0;x',y',H_0) \\ &+ h(x,y;t)\partial_z G_{3D}(x,y,z;x',y',H_0)|_{z=H_0} \\ &+ h(x',y';t)\partial_{z'} G_{3D}(x,y,H_0;x',y',z')|_{z'=H_0}. \quad (15)\end{aligned}$$

Substituting this into the meniscus equation (14) gives

$$I_A = \sigma_B \partial_y^2 H_0, \quad I_B + I_C + I_D + I_E + I_F = \sigma_B \nabla^2 h(x,y;t), \quad (16)$$

where the left-hand side equation is to the zeroth order and the right-hand side is to the first order in $h(x,y,t)$ or $\delta Y(x,H_0)$. These terms are defined in the same fashion as those in the Cartesian coordinate system [19]. The terms I_E and I_F arise from the fluctuating wall. They are given by

$$I_A(x,y) \equiv \int dx_1 \int dy_1 G_{3D}(x,y,H_0(t);x_1,y_1,H_0(t))\partial_t H_0(t), \quad (17)$$

$$I_B(x,y) \equiv \int dx_1 \int dy_1 \partial_z G_{3D}(x,y,z;x_1,y_1,H_0(t))|_{z=H_0} \times h(x,y;t)\partial_t H_0(t), \quad (18)$$

$$I_C(x,y) \equiv \int dx_1 \int dy_1 \partial_{z_1} G_{3D}(x,y,H_0(t);x_1,y_1,z_1)|_{z_1=H_0} \times h(x_1,y_1;t)\partial_t H_0(t), \quad (19)$$

$$I_D(x,y) \equiv \int dx_1 \int dy_1 G_{3D}(x,y,H_0(t);x_1,y_1,H_0(t)) \times \partial_t h(x_1,y_1;t), \quad (20)$$

$$I_E(x,y) \equiv \int dx_1 \int dy_1 \partial_y G_{3D}(x,y,H_0(t);x_1,y_1,H_0(t)) \times \delta Y(x,H_0)\partial_t H_0(t), \quad (21)$$

$$I_F(x,y) \equiv \int dx_1 \int dy_1 \partial_{y_1} G_{3D}(x,y,H_0(t);x_1,y_1,H_0(t)) \times \delta Y(x_1,H_0)\partial_t H_0(t). \quad (22)$$

The zeroth-order equation would give the Washburn law, if we used the Green's function for the geometry between two walls and assumed a constant curvature for the meniscus. We will assume an average profile $H_0(t)$, which can be considered to obey Washburn's law even though we have only a single vertical wall in the system. Since H_0 is not needed for determining the form of the evolution equation for the fluctuating part h of Eq. (16) at that single wall, the precise time dependence of H_0 is not crucial for the analysis to be presented below.

A local equation of motion for the meniscus fluctuations can be obtained by Fourier-cosine transformation following [19]. The above terms become

$$\mathcal{F}_{x/k_x}\mathcal{F}^{\cos}_{y/k_y}[I_B] = \frac{1}{2}\dot{H}_0 h(\vec{k},t), \quad (23)$$

$$\mathcal{F}_{x/k_x}\mathcal{F}^{\cos}_{y/k_y}[I_C] = \frac{1}{2}e^{-2kH_0}\dot{H}_0 h(\vec{k},t), \quad (24)$$

$$\mathcal{F}_{x/k_x}\mathcal{F}^{\cos}_{y/k_y}[I_D] = \frac{1}{2k}\dot{h}(\vec{k},t)(1-e^{-2kH_0}), \quad (25)$$

$$I_E = 0, \quad (26)$$

$$\mathcal{F}_{x/k_x}\mathcal{F}^{\cos}_{y/k_y}[I_F] = \frac{\dot{H}_0(t)}{2k}(1-e^{-2kH_0})\delta Y(k_x,H_0(t)), \quad (27)$$

where $k = \sqrt{k_x^2 + k_y^2}$. We then have the meniscus equation of motion using the above in the Fourier transform of Eq. (16),

$$\partial_t h(\vec{k},t) = -\frac{k\partial_t H_0(t)(1+e^{-2H_0(t)k})+\sigma_B k^3}{(1-e^{-2H_0(t)k})}h(\vec{k},t) + k\dot{H}_0\delta Y(\vec{k},H_0). \tag{28}$$

The deterministic part of the above meniscus equation is identical to the deterministic part of the LIE derived from the 2D phase-field model (8), apart from the dimensionality. This is by construction, since the same method was used for the same theory in different dimensions by applying the corresponding Green's functions.

A similar analysis can also be performed for the case in which the disorder at the walls consists of chemical impurities (i.e., spatially fluctuating surface tension) instead of spatial roughness [19]. In this case, the deterministic part of the meniscus equation is by construction identical to that of the above. However, there is no effective noise at the meniscus level, since the effect of the disorder comes in from the contact line that serves as a boundary condition for the meniscus.

B. Contact line dynamics

To proceed to the level of the 1D contact line, we consider the generalized variational approach [19]. Formally, one can write the 3D phase-field model in terms of variations of a Rayleigh dissipation functional, and a free-energy functional. Then, using approximations that express higher-dimensional entities in term of the relevant lower-dimensional ones, we obtain a chain of projection equations as

$$\frac{\delta R_{3D}[\dot{\phi}]}{\delta\dot{\phi}(x,y,z;t)} = -\frac{\delta F_{3D}[\phi]}{\delta\phi(x,y,z;t)} \tag{29}$$

$$\Rightarrow \frac{\delta R_{2D}[\dot{H}]}{\delta\dot{H}(x,y;t)} = -\frac{\delta F_{2D}[H]}{\delta H(x,y;t)} \tag{30}$$

$$\Rightarrow \frac{\delta R_{1D}[\dot{C}]}{\delta\dot{C}(x;t)} = -\frac{\delta F_{1D}[C]}{\delta C(x;t)}, \tag{31}$$

where $R_{d\mathrm{D}}$ refers to the Rayleigh dissipation functional and $F_{d\mathrm{D}}$ refers to the free-energy functional in d-dimensional space. Here the relevant 3D, 2D, and 1D objects are the phase field, the meniscus profile, and the contact line profile, respectively. The variable $C(x;t)$ denotes the fluctuating contact line profile, and $H(x,y;t)=H_0(t)+h(x,y;t)$ is for the one-wall case. The corresponding expansion for the contact line is $C(x,t)=C_0(t)+c(x,t)$. For small fluctuations h and c, consistency requires that $C_0(t)=H_0(t)$. The projection from 3D to 2D is made possible by the 1D kink approximation in the direction normal to the interface, as demonstrated in the preceding section. The corresponding approximation we have used to make the 2D to 1D projection possible is the quasistationary (QS) approximation $\nabla^2 h(x,y;t)=0$; $h(x,0,t)=c(x,t)$, which corresponds to the minimum of energy constrained by the contact line profile. The meniscus can then be expressed in terms of the contact line as

$$h_{\mathrm{qs}}(x,y;t) = \int_{-\infty}^{\infty} dx_1 g(x-x_1,y)c(x_1;t), \tag{32}$$

$$g(k_x,y) = e^{-|k_x|y} \Leftrightarrow g(x,y) = \frac{1}{\pi}\frac{y}{x^2-y^2}. \tag{33}$$

The explicit forms for the Rayleigh dissipation and free-energy functionals that reproduce the meniscus equation (14) when plugged into Eq. (30) are

$$R_{2D}[\dot{H}] = \int_{-\infty}^{\infty} dx_1 dx_2 \int_0^{\infty} dy_1 dy_2 \int dt_1 \dot{H}(x_1,y_1,t_1) \times \tilde{G}_{3D}(x_1,y_1,H(x_1,y_1,t_1);x_2,y_2, H(x_2,y_2,t))\dot{H}(x_2,y_2,t_1), \tag{34}$$

$$F_{2D}[H] = \sigma_B \int_{-\infty}^{\infty} dx_1 \int_0^{\infty} dy_1 \int dt_1 \sqrt{1+|\nabla H(x_1,y_1,t_1)|^2}. \tag{35}$$

The effective 1D functionals can be obtained from the above by inserting the quasistationary approximation h_{qs} into Eqs. (34) and (35). In order to obtain the 1D equation of motion to linear order in small fluctuations, one needs to expand the functionals to second order in both $c(x,t)$ and $\delta Y(x,y)$, and then take the variation with respect to the contact line as shown in Eq. (31).

Neglecting the zeroth-order equation for the reasons mentioned earlier, the general Fourier space equation of motion we obtain for the first-order fluctuations is

$$\mathcal{F}_{x/k_x}[I_2+I_3+I_4+I_5+I_6] = -\sigma_B|k_x|c(k_x,t), \tag{36}$$

where the left-hand side is the variation of the Rayleigh dissipation functional and the right-hand side is the variation of the free energy. The right-hand side is recognized as the deterministic restoring force acting on the contact line [33]. The shorthand notations stand for

$$I_2(x) = 2\dot{C}_0 \int_{-\infty}^{\infty} dx_1 dx_2 dx_3 \int_0^{\infty} dy_1 dy_2 g(x-x_1,y_1) \times \partial_{z_1} G_{3D}(x_1,y_1,z_1;x_2,y_2,C_0)|_{z_1=C_0} g(x_1-x_3,y_1)c(x_3,t), \tag{37}$$

$$I_3(x) = 2\dot{C}_0 \int_{-\infty}^{\infty} dx_1 dx_2 dx_3 \int_0^{\infty} dy_1 dy_2 g(x-x_1,y_1) \times \partial_{z_2} G_{3D}(x_1,y_1,C_0;x_2,y_2,z_2)|_{z_2=C_0} g(x_2-x_3,y_2)c(x_3,t), \tag{38}$$

$$I_4(x) = 2\int_{-\infty}^{\infty} dx_1 dx_2 dx_3 \int_0^{\infty} dy_1 dy_2 g(x-x_1,y_1) \times G_{3D}(x_1,y_1,C_0;x_2,y_2,C_0) g(x_2-x_3,y_2)\dot{c}(x_3,t), \tag{39}$$

$$I_5(x) = 2\dot{C}_0 \int_{-\infty}^{\infty} dx_1 dx_2 \int_0^{\infty} dy_1 dy_2 g(x-x_1,y_1) \times \partial_{y_1} G_{3D}(x_1,y_1,C_0;x_2,y_2,C_0)\delta Y(x_1,C_0), \quad (40)$$

$$I_6(x) = 2\dot{C}_0 \int_{-\infty}^{\infty} dx_1 dx_2 \int_0^{\infty} dy_1 dy_2 g(x-x_1,y_1) \times \partial_{y_2} G_{3D}(x_1,y_1,C_0;x_2,y_2,C_0)\delta Y(x_2,C_0). \quad (41)$$

Not all of these integrals are solvable in closed form, but can be approximated to a good degree of accuracy by the following expressions:

$$\mathcal{F}_{x/k_x}[I_2] = \frac{\dot{C}_0}{2|k_x|} c(k_x,t), \quad (42)$$

$$\mathcal{F}_{x/k_x}[I_3] = \frac{2\dot{C}_0}{\pi|k_x|} c(k_x,t) \int_1^{\infty} ds \frac{e^{-2|k_x|C_0 s}}{s^3\sqrt{s^2-1}} \approx \frac{1.14\times 4}{3\pi|k_x|} \dot{C}_0 c(k_x,t) e^{-2.28|k_x|C_0}, \quad (43)$$

$$\mathcal{F}_{x/k_x}[I_4] = \frac{2\dot{c}(k_x,t)}{k_x^2\pi} \int_1^{\infty} ds \frac{1-e^{-2|k_x|C_0 s}}{s^4\sqrt{s^2-1}} \approx \frac{4\dot{c}(k_x,t)}{3\pi k_x^2}(1-e^{-2.28|k_x|C_0}), \quad (44)$$

$$\mathcal{F}_{x/k_x}[I_5] = 0, \quad (45)$$

$$\mathcal{F}_{x/k_x}[I_6] = \frac{2}{\pi|k_x|} \dot{C}_0 \delta Y(k_x,C_0) \int_1^{\infty} ds \frac{1-e^{-2|k_x|C_0 s}}{s^2\sqrt{s^2-1}} \approx \frac{2}{\pi|k_x|} \dot{C}_0 \delta Y(k_x,C_0)(1-e^{-2.56|k_x|C_0}). \quad (46)$$

We note that the corrections to the free-energy functional in the curvilinear coordinates are of third order in δY and h. This can be seen by coordinate transforming the area element, which in Cartesian coordinates is $\sqrt{1+(\nabla h)^2} \approx 1 + \frac{1}{2}(\nabla h)^2$.

Finally, after approximating $\frac{1.14\times 4}{3\pi} \approx \frac{1}{2}$ and $\frac{(1-e^{-2.56|k_x|C_0})}{(1-e^{-2.28|k_x|C_0})} \approx 1$, the equation of motion for the contact line fluctuations becomes

$$\dot{c}(k_x,t) = -\frac{\frac{3\pi|k_x|\dot{C}_0}{8}(1+e^{-2.28|k_x|C_0}) + \sigma_B|k_x|^3}{(1-e^{-2.28|k_x|C_0})} c(k_x,t) + \frac{3}{2}|k_x|\dot{C}_0\delta Y(k_x,C_0). \quad (47)$$

Note that all of the approximations above are for dimensionless quantities, with errors depending on the physical parameter $|k_x|C_0$. The relative errors in the approximated functional forms are under 3%, when compared against numerical integration of the respective integrals for different values of $|k_x C_0|$. An exception to this are relative errors of $\mathcal{F}_{x/k_x}[I_4]$ and $\mathcal{F}_{x/k_x}[I_6]$ when $|k_x| \to 0$, as both I_4 and I_6 vanish at the limit, causing the relative error to be high. However, at machine precision away from $|k_x|=0$, these errors are no more than 15%, and more importantly the error of the complete dispersion relation stays within the 3% error margin. This is due to the fact that the dispersion goes to a positive constant when $|k_x| \to 0$, as one can see from Fig. 1.

Apart from simple numerical factors, the contact line equation above has the same functional form as the results derived in the previous sections. In particular, $\partial_t h = -(\sigma|k_x|^3 + \dot{H}_0|k_x|)h$ in the "deep" limit $k_x^{-1} \ll H_0(t)$, which thus agrees with the previous works discussed earlier [11,23,31]. This form of dispersion relation is always obtained by our method for interfaces in model *B*. This has to do with the quasistationary approximation, which essentially assumes that meniscus fluctuations dampen quickly in the direction perpendicular to the contact line, in order to obtain temporally local equations. How this leads to the coupling of the meniscus and contact line dynamics is discussed in more detail in another publication [20].

The effective noise term we obtain from the 3D model shares the property of linear dependence on the velocity of the propagation with the 2D mobility noise, and with the previous analyses [11,23,31]. In the case of surface tension impurities at the wall [19], the effective contact line noise is proportional to k_x^2, whereas in the fluctuating wall case in Eq. (47) the $|k_x|$ dependence is linear. This is analogous to the 2D mobility disorder in the sense that the effective noise here is different from that obtained for conserved disorder. The extra factor of $|k_x|$ as compared to the 2D model [Eq. (8)] comes from the fact that the disorder in the 3D model comes from the walls, whereas in the 2D model the disorder is in the bulk. Or in other words, the term $|k_x|\delta Y(k_x,C_0)$ has the same dimensionality as $\xi(k)$ in the 2D case in Eq. (10).

We note that the more complicated properties of the noise in the form of nonlocality in Fourier space are lost by our approximations. Note that the noise is still nonlocal in real space, as is apparent from its real-space representation I_6 in Eq. (41). In addition to Fourier space nonlocalities, our one-wall approach does not explicitly include the gap spacing, which provides an additional physical length scale [36]. Likely due to this, our resulting noise term shows similarities to, but does not quantitatively agree with, the noise terms of Ref. [11], where the gap fluctuations were considered as the source of disorder in the context of Darcy's law and capillarity. This will be discussed in greater length below.

IV. DISCUSSION AND CONCLUSIONS

In this paper, we have studied the effective interface dynamics of the three-phase contact line in a Hele-Shaw experiment by deriving the meniscus and contact line equations of motion from higher-dimensional bulk phase-field theories by projection methods. The projection methods take into account the nonlocal dynamics of the system caused by local mass conservation, and can be systematically applied starting

from a full 3D description. We have considered here two particular models, namely an ad hoc model where the disorder is in the effective mobility in 2D [26], and a more microscopic model where wall corrugation in 3D is explicitly treated with a curvilinear coordinate transformation. In both cases, we have focused on the limit of small disorder by linearizing in disorder strength and in the fluctuations caused by the disorder. By construction this linearization, performed in real space, causes the Fourier space representations of the equations of motion to be local. The upside of this is that the effective dynamics are written in a concise manner, and the physical predictions are relatively easily interpreted and the equations we obtain are readily affable to numerical analysis. The obvious downside is that the procedure involves a number of approximations, the validity of which is not certain *a priori*.

In particular, the quasistationary approximation of Eq. (32), which ultimately enables our contact line analysis, requires a critical assessment. A more rigorous approach would in fact consider the contact line as the boundary condition to the meniscus equation of motion (28). However, explicitly solving the meniscus profile as a function of the contact line leads to an equation that is, among other things, nonlocal in time. Thus we are forced to simplify the model by using the QS approximation, the validity of which we can consider both from a physical perspective, or more rigorously by considering the limits of the meniscus equation of motion. Physically, the QS approximation comes from the minimum of meniscus energy constrained by the boundary condition of the contact line. This is expected to define the meniscus profile when the meniscus moves slowly, and thus it is called the quasistationary approximation. Mathematically, the meniscus equation (28) reduces to the diffusion equation when $C_0 \ll k^{-1} \ll \sqrt{\sigma/\dot{C}_0}$ and $\partial_t h(x,y,t) \approx 0$. In this limit, the meniscus level disorder I_F acts as a source term,

$$\sigma_B \nabla^2 h(x,y;t) = I_F. \tag{48}$$

This leads to an additional disorder term in the QS approximation, which then leads to a plethora of new first-order disorder terms in R_{1D} and F_{1D}. However, all these new disorder terms arising from R_{1D} are proportional to $\dot{C}_0^2$, and thus not relevant in the QS limit. Additionally, the two new disorder terms created in F_{1D} due to I_F cancel each other out exactly. Thus, we expect our results with the simplified version of the QS approximation to hold in this particular limit.

In addition to the detailed derivations and new projection formalism presented here, our purpose has been quantitatively to compare two different approaches to modeling rough wall Hele-Shaw experiments, namely that based on the 2D phase-field model with a stochastic mobility, Eq. (2), and the 3D phase-field model with a fluctuating geometry. The projection method we use for both cases produces the linear response of the meniscus and contact line to small fluctuations. For both cases, the k dependence of the meniscus and contact line deterministic LIEs is the same. In particular, in the special case of the "deep" limit where $k^{-1} \ll H_0(t)$, the asymptotic forms of our general dispersion relations are in agreement with previous works on the Hele-Shaw problem by Pauné and Casademunt [11], Ganesan and Brenner [31], and Hernández-Machado *et al.* [23]. The main advantage of our projection formalism is the way it incorporates the noise into the projection, and thus allows us to study the effective noise caused to the contact line level by bulk or wall disorder. The main result of this analysis is that in both cases the effective noise is linearly proportional to the velocity of the interface. While this result agrees qualitatively with the other works cited above, quantitative differences remain in the form of the noise terms. The relevance of these differences to the actual kinetic roughening of the interfaces remains a challenging numerical problem.

In comparison with the work of Pauné and Casademunt, our effective noise in Eq. (9) behaves similarly to the permeability and bulk noises of Ref. [11] depending on the noise correlation length and the magnitude of the wave vector k_x. When comparing our 3D result to Ref. [11], one must consider the issue of the gap spacing. In Ref. [11], the authors consider disorder in the gap spacing as a fraction of the average gap spacing, b_0, whereas in our model the disorder is independent of the gap spacing, and only the large gap limit is considered. Our 3D effective noise seems not to conform exactly to either the permeability or the capillary noise, even though it has elements from both. Even though the noise term in Eq. (47) looks like the capillary noise of Pauné and Casademunt as what comes to the linear $|k_x|$ dependence, it is different because we have the mean velocity $\dot{C}_0$ multiplying the noise term. This velocity dependence is similar to that of the permeability noise, compared to which our noise has an extra factor of $|k_x|$. Furthermore, in the limit of $b_0 \to \infty$, the real capillary noise should vanish if the curvature vanishes. Direct comparison is difficult, however, as taking the infinite gap spacing $b_0 \to \infty$ while keeping the gap variations constant is not the limit at which Eq. (6) of Ref. [11] is meant to be valid. Thus the discrepancies likely originate from the large gap limit, implying that there is yet another noise regime when the gap is large compared to wall fluctuations. Another possibility is that including the gap fluctuations as effective permeability might not be faithful enough a representation to give the correct effective noise for a Hele-Shaw cell with fluctuating walls. This was one of the main questions we originally set out to investigate in this work. Because of the large gap limit, we can only state that we could not clearly verify that wall fluctuations could be effectively described by permeability, or mobility, disorder.

Our method of transformation to fluctuating coordinates offers a possible route to clarify the noise source issues discussed above. This is because the gap disorder is explicitly accounted for as a fluctuating wall, as opposed to inserting noise into phenomenological, mesoscopic quantities such as capillarity [11,16], permeability in Darcy's law [11], or mobility in the phase-field model [23]. The case of a Hele-Shaw cell where the wall fluctuations are comparable in size to the gap thickness could be analyzed by this method. One would then need to use the 3D Green's function of a geometry that is constrained by two parallel walls. In addition to this, one would need to consider two coupled contact lines in the QS approximation. The coordinate transformation would involve a shift and a rescale to give two walls, which appear straight.

All this makes the calculation significantly more involved, and the convolutions over the Green's functions might not be so readily expressible in Fourier space. The comparison of these results to the different effective noise terms obtained by Pauné and Casademunt in Ref. [11] would be very interesting, however. One can readily see from our approach that different types of disorder arise at the linearized level from the wall fluctuations. In particular, the coordinate transformation would include a nonunity Jacobian (the rescale), which is explicitly the "nonconserved 2D volume" considered in Ref. [11]. Unfortunately, such a calculation is beyond the scope of this paper.

ACKNOWLEDGMENTS

We would like to thank K. Elder for inspirational and pleasant discussions, as well as for sharing his expertise and results on the sharp interface analysis. This work has been supported in part by the Academy of Finland through its Center of Excellence grant (COMP). S.M. has been supported by a personal grant from the Academy of Finland.

APPENDIX: CURVILINEAR COORDINATE SYSTEM BY FLUCTUATING WALL

In this appendix, we will consider in more detail the Green's function of the Laplacian in the fluctuating coordinate system

$$x' = x, \quad y' = y - \delta Y(x,z), \quad z' = z, \tag{A1}$$

which is schematically depicted in Fig. 2. The generalization to the two-wall setup is straightforward but very tedious, including two independent disorder functions. In particular, we will consider the correction to the Green's function to linear order in small wall fluctuations $\delta Y(x,z)$. First, the metric tensor of the above coordinate system can be obtained by transformation of the Cartesian metric tensor as

$$[g_{i'j'}] = \sum_i \frac{\partial x^i}{\partial x^{i'}} \frac{\partial x^i}{\partial x^{j'}} = \begin{bmatrix} 1 + (\partial_x \delta Y)^2 & \partial_x \delta Y & \partial_z \delta Y \partial_x \delta Y \\ \partial_x \delta Y & 1 & \partial_z \delta Y \\ \partial_z \delta Y \partial_x \delta Y & \partial_z \delta Y & 1 + (\partial_z \delta Y)^2 \end{bmatrix}. \tag{A2}$$

The coordinate transformation from Cartesian coordinates is merely a shift, and thus the integration measure should not change, meaning that the Jacobian in the coordinate transformation of an integral should be unity. This is indeed so, since

$$\det([g_{i'j'}]) \equiv 1. \tag{A3}$$

In the case of Cartesian coordinates, we can obtain the Green's function, which we denote G_{3D}, using the image charge method with the Dirichlet boundary condition at $z=0$ and the Neumann boundary condition at $y=0$,

$$G_{3D} = G_{3D}^{+} + G_{3D}^{-}, \tag{A4}$$

$$G_{3D}^{\pm} = \frac{1}{4\pi}\left[\frac{1}{\sqrt{(x-x_1)^2 + (y \pm y_1)^2 + (z-z_1)^2}} - \frac{1}{\sqrt{(x-x_1)^2 + (y \pm y_1)^2 + (z+z_1)^2}} \right]. \tag{A5}$$

We work in the limit of small fluctuations, so we write the Laplacian in the curvilinear coordinates as the Cartesian Laplacian plus a correction, $\tilde{\nabla}^2 = \nabla^2 + L$. Note that we unconventionally denote $\nabla^2 = \partial_{x_1}^2 + \partial_{x_2}^2 + \partial_{x_3}^2$ for any coordinates $[x_1, x_2, x_3]$. The correction L is explicitly shown below,

$$L = 2\left[\frac{\partial \delta Y(x,z)}{\partial x}\right]\frac{\partial^2}{\partial x \partial y} + 2\left[\frac{\partial \delta Y(x,z)}{\partial z}\right]\frac{\partial^2}{\partial z \partial y} + \left[\frac{\partial^2 \delta Y(x,z)}{\partial x^2} + \frac{\partial^2 \delta Y(x,z)}{\partial z^2}\right]\frac{\partial}{\partial y}. \tag{A6}$$

In order to use Eq. (12) for the curvilinear coordinates, we need the Green's function, which has the property of $[\nabla'^2 + L']\tilde{G}_{3D}(\boldsymbol{r}', \boldsymbol{r}_1') = -\delta(\boldsymbol{r}' - \boldsymbol{r}_1')$. Since the Laplacian in the curvilinear coordinates can be expressed as the Cartesian Laplacian plus a correction, we can find the inverse of the curvilinear Laplacian, or $\tilde{G}_{3D}$, to first order in δY as

$$\tilde{G}_{3D}(\boldsymbol{r}', \boldsymbol{r}_1') \cong (\nabla'^2)^{-1} - (\nabla'^2)^{-1} L' (\nabla'^2)^{-1}. \tag{A7}$$

The above operator notation can be written in full form as

$$\tilde{G}_{3D}(\boldsymbol{r}'; \boldsymbol{r}_1') \approx G_{3D}(\boldsymbol{r}'; \boldsymbol{r}_1') - \int_{-\infty}^{\infty} dx_2 \int_0^{\infty} dy_2 \int_0^{\infty} dz_2 G_{3D} \times (\boldsymbol{r}'; \boldsymbol{r}_2') L(\boldsymbol{r}_2') G_{3D}(\boldsymbol{r}_2'; \boldsymbol{r}_1'). \tag{A8}$$

Substituting G_{3D} into the above, we can work out the correction to the Green's function. After using a similar argument to neglect surface integrals of the type $\int dx' G(x, H(x,t); x', 0)\xi(x')$ as we did with Eq. (4), we find

$$\tilde{G}_{3D}(\boldsymbol{r}_1'; \boldsymbol{r}_2') = G_{3D}(\boldsymbol{r}_1'; \boldsymbol{r}_2') - \delta Y(\boldsymbol{r}_1') \partial_{y_1'} G_{3D}(\boldsymbol{r}_1'; \boldsymbol{r}_2') - \delta Y(\boldsymbol{r}_2') \partial_{y_2'} G_{3D}(\boldsymbol{r}_1'; \boldsymbol{r}_2'). \tag{A9}$$

At this point, the primes can just be dropped, since $\partial_y = \partial_{y'}$. This result is hardly surprising, since a simple substitution of $y' = y - \delta Y(x,z)$ to $G_{3D}(\boldsymbol{r}_1', \boldsymbol{r}_2')$ yields identical results to linear order.

The neglected surface integrals include a reservoir term and a wall term. The reservoir term can be readily seen to be small when the meniscus is farther away from the reservoir than the disorder correlation length. Additionally, the reservoir boundary correction is zero when considering columnar, i.e., z-independent disorder. The wall term is more problematic, since it involves the boundary correction due to fluctuation in the direction of the wall normal. We have to observe the meniscus farther away from the wall than the disorder correlation length in order to neglect this boundary correction. The absence of boundary disorder corrections is highly desirable if we are to keep our formalism tractable, so we have neglected the boundary corrections to the Green's function.

[1] D. Moldovan and L. Golubovic, Phys. Rev. E **61**, 6190 (2000).
[2] J. P. Bouchaud and A. Georges, Phys. Rep. **195**, 127 (1990).
[3] A. E. Scheidegger, *The Physics of Flow through Porous Media* (MacMillan Co., New York, 1957).
[4] J. Krug, Adv. Phys. **46**, 139 (1997).
[5] S. Moulinet, A. Rosso, W. Krauth, and E. Rolley, Phys. Rev. E **69**, 035103(R) (2004).
[6] J. F. Joanny and M. O. Robbins, J. Chem. Phys. **92**, 3206 (1990).
[7] D. Ertas and M. Kardar, Phys. Rev. E **49**, R2532 (1994).
[8] A.-L. Barabási and H. E. Stanley, *Fractal Concepts in Surface Growth* (Cambridge University Press, Cambridge, 1995).
[9] J. Maunuksela *et al.*, Phys. Rev. Lett. **79**, 1515 (1997); M. Myllys *et al.*, *ibid.* **84**, 1946 (2000); , Phys. Rev. E **64**, 036101 (2001).
[10] J. Soriano, J. Ortín, and A. Hernández-Machado, Phys. Rev. E **66**, 031603 (2002); **67**, 056308 (2003).
[11] E. Pauné and J. Casademunt, Phys. Rev. Lett. **90**, 144504 (2003).
[12] D. Geromichalos, F. Mugele, and S. Herminghaus, Phys. Rev. Lett. **89**, 104503 (2002).
[13] S. V. Buldyrev *et al.*, Phys. Rev. A **45**, R8313 (1992).
[14] V. K. Horváth and H. E. Stanley, Phys. Rev. E **52**, 5166 (1995).
[15] L. A. N. Amaral *et al.*, Phys. Rev. Lett. **72**, 641 (1994).
[16] M. Dubé *et al.*, Phys. Rev. Lett. **83**, 1628 (1999); Eur. Phys. J. B **15**, 701 (2000); Phys. Rev. E **64**, 051605 (2001).
[17] T. Laurila, C. Tong, I. Huopaniemi, S. Majaniemi, and T. Ala-Nissila, Eur. Phys. J. B **46**, 553 (2005).
[18] K. R. Elder, M. Grant, N. Provatas, and J. M. Kosterlitz, Phys. Rev. E **64**, 021604 (2001).
[19] S. Majaniemi, Ph. D. thesis, Helsinki University of Technology, Finland (2004). http://lib.tkk.fi/Diss/2004/isbn9512270897/
[20] S. Majaniemi, K. R. Elder, C. Tong, T. Laurila, and T. Ala-Nissila (unpublished).
[21] J. Asikainen, S. Majaniemi, M. Dubé, J. Heinonen, and T. Ala-Nissila, Eur. Phys. J. B **30**, 253 (2002).
[22] J. J. Ramasco, J. M. López, and M. A. Rodríguez, Phys. Rev. Lett. **84**, 2199 (2000).
[23] A. Hernández-Machado, J. Soriano, A. M. Lacasta, M. A. Rodríguez, L. Ramírez-Piscina, and J. Ortín, Europhys. Lett. **55**, 194 (2001).
[24] M. Dubé, B. Chabot, C. Daneault, and M. Alava, Pulp Paper Canada **106**, 24 (2005).
[25] J. D. Anderson Jr., *Computational Fluid Dynamics: The Basics with Applications* (McGraw-Hill, New York, 1995).
[26] A. Hernández-Machado, A. M. Lacasta, E. Mayoral, and E. C. Poiré, Phys. Rev. E **68**, 046310 (2003).
[27] K. Kawasaki and T. Ohta, Prog. Theor. Phys. **68**, 129 (1982).
[28] T. Ala-Nissila, S. Majaniemi, and K. Elder, Lect. Notes Phys. **640**, 357 (2004).
[29] M. Alava, M. Dubé, and M. Rost, Adv. Phys. **53**, 83 (2004).
[30] A. J. Bray, Adv. Phys. **43**, 357 (1994).
[31] V. Ganesan and H. Brenner, Phys. Rev. Lett. **81**, 578 (1998).
[32] R. K. P. Zia, Nucl. Phys. B **251**, 676 (1985).
[33] J. F. Joanny and P. G. de Gennes, J. Chem. Phys. **81**, 552 (1984).
[34] The term $\partial_u \mu$ is approximated with its form for the 1D disorder-free system: $\partial_u \mu \approx \frac{v_n}{M}\Theta(u)$, where v_n is the normal velocity. This approximation is similar to the 1D kink solution in the standard procedure, but its range of extent is not only near the interface, but between the reservoir and interface. Another assumption we made in the derivation is neglecting boundary terms of the form $\int dx' G(x, H(x,t); x', 0)\xi(x')$. This is justified when the width of the Kernel G along x direction, which is of order H, is much larger than the correlation length of the disorder ξ.
[35] We note that these associations are not consistent with the linearization in small disorder, since different orders in an expansion should be kept separate. However, the agreement between the long-wavelength in linear order and the zeroth order means that the same physical effect, namely mass transport, both drives the propagation and dissipates long-wavelength fluctuations. This will not be the case when the flow is forced, however.
[36] By using the Green's function of the two-wall geometry, it would be a possible but an extremely lengthy calculation to take the gap spacing explicitly into account in our model, but the result would be two coupled equations of motion.